Notch3 mediated TGF-β1 activation enhances epithelial-mesenchymal transition and cancer stemness in non-small lung cancer

FANG WANG[1*], SIQI HU[1*], JIANGRONG BIAN[1], QING GAO[1,2], LIUZHAO CAO[1], LINLI SANG[1], JUNJUN YANG[1] and XINGXIANG XU[1]

[1]Department of Respiration and Critical Care Medicine, Northern Jiangsu People's Hospital Affiliated to Yangzhou University, Yangzhou, Jiangsu 225001, P.R. China; [2]Department of Respiration and Critical Care Medicine, Yantai Affiliated Hospital of Binzhou Medical University, Yantai, Shandong 256603, P.R. China

Received March 24, 2025; Accepted July 14, 2025

DOI: 10.3892/ijo.2025.5791

Abstract. Notch3 is a key regulator in various cancers, playing a crucial role in maintaining stemness and promoting epithelial-mesenchymal transition (EMT). However, its differential expression and regulatory mechanisms in non-small cell lung cancer (NSCLC) and cancer stem cells remain poorly understood. To investigate this, the present study examined Notch3 expression in NSCLC through Oncomine, The Cancer Genome Atlas and Gene Expression Omnibus databases and validated the results with immunohistochemistry, reverse transcription-quantitative PCR and western blotting. EMT was induced by TGF-β1 in NSCLC cells and functional assays (Transwell, wound healing and sphere formation) were performed to assess cellular changes. *In vivo* experiments using a xenograft mouse model were conducted to evaluate tumor growth and metastasis. The results showed that high Notch3 expression was associated with poor prognosis in NSCLC patients. Downregulation of Notch3 inhibited TGF-β1-induced EMT and CSC characteristics, resulting in reduced tumorigenic potential, whereas overexpression of the Notch3 intracellular domain enhanced these effects. Silencing Notch3 suppressed EMT and markedly inhibited tumor growth and metastasis *in vivo*. These findings demonstrated that Notch3 regulated EMT and CSC properties in NSCLC, promoting tumor recurrence and metastasis. Notch3 thus represents a promising therapeutic target and prognostic marker for NSCLC.

Correspondence to: Dr Xingxiang Xu or Dr Junjun Yang, Department of Respiration and Critical Care Medicine, Northern Jiangsu People's Hospital Affiliated to Yangzhou University, 28 Nan Tong Road, Yangzhou, Jiangsu 225001, P.R. China
E-mail: xuxx63@126.com
E-mail: xiaojun-87624@126.com

*Contributed equally

Key words: Notch3, cancer stem-like cells, epithelial-mesenchymal transition, non-small lung cancer

Introduction

Lung cancer is the most common malignant tumor and one of the deadliest cancers worldwide. The 5-year survival rate for lung cancer is only ~20% (1). It includes two major types: Small cell lung cancer (SCLC) and non-small cell lung cancer (NSCLC). NSCLC is the most common subtype of lung cancer, accounting for ~80% of all lung cancer cases (2). Although various strategies have been developed to treat NSCLC, including surgical resection, chemotherapy and/or radiotherapy, most NSCLC patients exhibit poor tolerance to chemotherapy and radiotherapy (3). Consequently, surgery remains the preferred option for early-stage disease and platinum-based chemotherapy is still the standard treatment protocol (3). Therefore, further research is needed to explore the mechanisms underlying the malignant behaviors in NSCLC.

Emerging research indicates that epithelial-mesenchymal transition (EMT) plays a critical role in tumorigenesis and metastasis (4,5). During the EMT process, epithelial tumor cells undergo significant morphological and phenotypic changes, including the loss of tight junctions, disappearance of cell polarity and reorganization of the cytoskeleton, endowing the cells with more invasive properties and phenotypic characteristics (6,7). Through EMT, cancer cells not only acquire resistance to apoptosis and chemotherapeutic drugs but may also develop stem cell-like properties (4,8). Cancer stem cells (CSCs) are also regarded as potential drivers of tumor initiation and progression (9,10). CSCs constitute a small portion of the cancer cell population and possess the unique ability to self-renew and generate more differentiated cells, which can give rise to new tumors (11,12). Studies have found that EMT is a factor that can induce CSC characteristics. CSCs are among the key factors contributing to cancer recurrence, metastasis and drug resistance (4,8,11). There is an intrinsic link between EMT and CSCs, and they are collectively implicated in tumor metastasis (4,8,13).

The human Notch signaling pathway consists of four receptors (Notch1-4) and five ligands (Jagged1-2, delta-like 1, 3 and 4) (14). Upon binding with its ligand, Notch releases the Notch intracellular domain (NICD). The NICD then translocates to the nucleus and regulates the transcription of target genes (15). The Notch signaling pathway plays pivotal roles in cell proliferation, stemness and invasion of NSCLC (16). In genetically engineered mouse models, the induced expression of Notch3 increases the tumorigenicity of the lungs (17). Inhibition of Notch3 expression reduces malignancy both *in vitro* and *in vivo* by inducing apoptosis and decreasing cell proliferation, migration and invasiveness (18). Studies have shown that high activation of Notch3 is associated with poor prognosis in lung cancer patients (19-21). Notch3 has been found to be associated with EMT and CSCs and is a potential therapeutic target for lung cancer (19,22). Additionally, when Notch3 expression is knocked down using small interfering RNA (siRNA), the proliferation of non-small lung cancer cells is also inhibited (22).

The present study investigated the involvement of Notch3 in EMT and CSCs of lung cancer and the relationship between Notch3 and TGF-β1. It found that reducing Notch3 expression effectively impeded the proliferation, metastasis and invasion of lung cancer cells, as demonstrated by *in vitro* and *in vivo* assays. However, how Notch3 influences EMT and CSCs in lung cancer cells is not fully elucidated. TGF-β1 was found to induce EMT and stemness features and this effect could be inhibited when Notch3 was knocked down in the lung cancer cells. The findings emphasized the critical role of Notch3 in the progression of NSCLC and propose Notch3 as a potential therapeutic target for NSCLC.

Materials and methods

Cell culture. The human NSCLC A549 (RRID:CVCL_0023), H1299 (RRID:CVCL_0060), H460 (RRID:CVCL_0459), H1975 (RRID:CVCL_1511) and H2170 (RRID:CVCL_1575) cell lines, along with the normal human bronchial epithelial cell line (BEAS-2B; RRID:CVCL_0168), were from Procell Life Science & Technology Co., Ltd. and maintained in appropriate medium supplemented with 10% fetal bovine serum (FBS; Wuhan Pricella Life Science and Technology Co., Ltd.) and 50 μg/ml penicillin-streptomycin (Gibco; Thermo Fisher Scientific, Inc.) in the appropriate conditions. Recombinant human TGF-β1 was from PeproTech, Inc. and stored as recommended.

Online data acquisition and analysis. Gene Expression Profiling Interactive Analysis (GEPIA; http://gepia.cancer-pku.cn) was used to predict the levels of gene expression in NSCLC and normal tissues. It was also employed to assess the correlation between genes. Protein-protein interaction (PPI) networks were constructed using the STRING database (http://string.embl.de/). Using the Kaplan-Meier plotter (http://kmplot.com/analysis/), the relationship between Notch3 expression and survival in lung cancer was examined. Additionally, the log-rank P-value and the hazard ratio (HR) with 95% confidence intervals were calculated.

Western blot (WB) analysis. Proteins were extracted from cells with RIPA buffer (Beijing Solarbio Science & Technology Co., Ltd.) with 1 mM PMSF protease inhibitor (MedChemExpress) added. A BCA Protein Assay Kit (Beyotime Institute of Biotechnology) was used to determine the concentration of total proteins in accordance with the manufacturer's instructions. A total of 40 μg protein was separated by 10% SDS-PAGE and then transferred to polyvinylidene difluoride membranes (MilliporeSigma). After the membranes were blocked with 5% milk (Beyotime Institute of Biotechnology) in tris-buffered saline containing 0.1% Tween-20 (TBST) at room temperature for 1 h and then incubated at 4˚C overnight with primary antibodies, including anti-Notch3-antibody (1:2,000; cat. no. CL488-55114; Proteintech Group, Inc.), anti-GAPDH antibody (1:10,000; cat. no. 60004-1-Ig; Proteintech Group, Inc.), anti-Vimentin (VIM) antibody (1:10,000; cat. no. 10366-1-AP; Proteintech Group, Inc.), anti-E-Cadherin antibody (1:5,000; cat. no. 31863-1-AP; Proteintech Group, Inc.), anti-β-actin antibody (1:2,000; cat. no. 60008-1-Ig; Proteintech Group, Inc.), anti-ALDH1A1 antibody (1:10,000; cat. no. 83830-2-RR; Proteintech Group, Inc.), anti-OCT4 antibody (1:2,000; cat. no. 60242-1-Ig; Proteintech Group, Inc.), anti-CD44 antibody (1:2,000; cat. no. 60224-1-Ig; Proteintech Group, Inc.) and anti-CD133 antibody (1:2,000; cat. no. 18470-1-AP; Proteintech Group, Inc.). The next day, the protein was washed with TBS-0.1% Tween three times and then incubated with secondary antibodies conjugated with horseradish peroxidase conjugated goat anti-rabbit IgG (1:10,000; cat. no. SA00001-2; Proteintech Group, Inc.) or anti-mouse IgG (1:10,000; cat. no. SA00001-1; Proteintech Group, Inc.) for 1 h at room temperature and then visualized by ECL detection kit (cat. no. BMU102-CN; Abbkine Scientific Co., Ltd.). Protein visualization was performed using ECL HRP substrate (cat. no. 34580; Thermo Fisher Scientific, Inc.). Images were captured using the BIO-RAD ChemiDoc MP multifunctional chemicalimaging instrument (Bio-Rad Laboratories, Inc.). The expression of protein was analyzed by ImageJ software (ImageJ 2.0; National Institutes of Health).

Reverse transcription-quantitative (RT-q) PCR. Total RNA was extracted from the cells using the FreeZol reagents (cat. no. R711-01; Vazyme Biotech Co., Ltd.) according to the manufacturer's instructions. The RNA concentration was measured using a Nano Drop ONE spectrophotometer (Thermo Fisher Scientific, Inc.). cDNA was performed according to the manufacturer's protocol using 1 μg total RNA and PrimerScript RT reagent kit (cat. no. R222-01; Vazyme Biotech Co., Ltd.). RT-qPCR was performed with SYBR Green Master Mix (cat. no. Q412-02; Vazyme Biotech Co., Ltd.). The thermocycling conditions were as follows: Initial denaturation at 95˚C for 30 sec. Denaturation at 95˚C for 10 sec, annealing and extension at 60˚C for 30 sec, 40 cycles. All reactions were conducted in a 20 μl reaction volume in triplicate. The primers used in these experiments are listed in Table I. The relative level of RNA was normalized to that of GAPDH using the $2^{-\Delta\Delta Cq}$ method (23).

Lentiviral and plasmid transfection. The 3rd generation system was used to generate lentivirus. Recombinant packaging plasmids (PG-P1-VSVG, PG-P2-REV and PG-P3-RRE) and vector plasmids (lentivirus vector) were prepared by Shanghai GenePharma Co., Ltd. A total of 1 μg

Table I. Primers used for PCR amplification.

Gene	Forward, 5'→3'	Reverse, 5'→3'
Notch3	CGTGGCTTCTTTCTACTGTGC	CGTTCACCGGATTTGTGTCAC
OCT4	GGGAGATTGATAACTGGTGTGTT	GTGTATATCCCAGGGTGATCCTC
EpCAM	TGATCCTGACTGCGATGAGAG	CTTGTCTGTTCTTCTGACCCC
Nanog	TTTGTGGGCCTGAAGAAAACT	AGGGCTGTCCTGAATAAGCAG
SOX2	TACAGCATGTCCTACTCGCAG	GAGGAAGAGGTAACCACAGGG
CD133	AGTCGGAAACTGGCAGATAGC	GGTAGTGTTGTACTGGGCCAAT
ABCG2	CAGGTGGAGGCAAATCTTCGT	ACCCTGTTAATCCGTTCGTTTT
E-Cadherin	CGAGAGCTACACGTTCACGG	GGGTGTCGAGGGAAAAATAGG
Vimentin	AGTCCACTGAGTACCGGAGAC	CATTTCACGCATCTGGCGTTC
GAPDH	CTCACCGGATGCACCAATGTT	CGCGTTGCTCACAATGTTCAT

third generation lentiviral packaging system package mix was prepared in the ratio of PG-P1-VSVG: PG-P2-REV: PG-P3-RRE 1:2:3 for the lentiviral plasmid packaging experiments in 60-mm cell culture dishes. RNAi-Mate (cat. no. GO4001; Shanghai GenePharma Co., Ltd.) to co-transfect 293T cells (Shanghai GenePharma Co., Ltd.). Cells were incubated at 37˚C with 5% CO_2 for 48 h post-transfection. After 48 h, the viral supernatant was collected, filtered through a 0.45-μm filter and concentrated by ultracentrifugation at 73,000 x g for 2 h at 4˚C. ShNotch3-containing plasmid backbone was LV3(H1/GFP&Puro) and its sequence was 5'-AGATCTGGCACCCTGACTTAT-3'. Sequence of shSUCLG1 negative control was 5'-TTCTCCGAACGT GTCACGT-3'. Short hairpin (sh)RNA sequences used were shRNA sequence targeting Notch3: Sh-Notch3-1:5'-GGG TTTGAGGGTCAGAATTGT-3', Sh-Notch3-2:5'-GATGCT ATCTGTGACACAAAT-3', Sh-Notch3-3:5'-GCTTGGGAA ATCAGCCTTACA-3'; and a scrambled shRNA sequence (5'-TTCTCCGAACGTGTCACGT-3') was used as control. A549 and H1975 cells (5x10^5 cells/well) were seeded in six-well plates and cultured for 24 h at 37˚C to reach 80% confluence. Lentiviral particles were mixed with polybrene (8 μg/ml) at a multiplicity of infection of 50, then added to cells and incubated at 37˚C for 48 h. Puromycin (1 μg/ml) was added 72 h post-transfection to facilitate screening of stably infected cells and 2-3 days later for subsequent experiments (1 μg/ml puromycin used for maintenance). For Notch3 overexpression, the pCLE Notch3 intracellular domain (N3ICD) over (pCLE NICD3, RRID: Addgene-26894) was purchased from Addgene, Inc. Cells were transfected with 2.5 μg NICD3 plasmid per well (six-well plate) using Lipofectamine® 3000 with Opti-MEM (cat. no. 31985-062; Invitrogen; Thermo Fisher Scientific, Inc.) in a biological safety cabinet, based on the kit's instructions. After 6 h of incubation at 37˚C, the medium was replaced with fresh complete culture medium. A total of 48 h after infection, the transfection efficiency was confirmed by RT-qPCR and WB.

Enzyme linked immunosorbent (ELISA) assay. The levels of TGF-β1 in the culture were measured using an ELISA kit (cat. no. EK0513; Boster Biological Technology, Ltd.), following the manufacturer's guidelines.

Cell counting kit-8 (CCK-8) assay. Lung cancer cells were cultured in 96-well plates (2,000 cells/well). According to the manufacturer's instructions, 10 μl of CCK-8 solution was added to each well and incubated at 37˚C for 3 h. Absorbance at 450 nm was measured.

Wound healing assay. A549 and H1975 cells were seeded into 6-well plates. When cells reached 90-95% confluence, the monolayer was scraped with a sterile 100 μl pipette tip and dislodged cells were removed with PBS. The cells were cultured in serum-free medium at 37˚C for 48 h, and images were acquired using a Zeiss light microscope (Carl Zeiss AG). The wound area at the same location was subsequently measured by ImageJ (V1.54d, National Institutes of Health). The cell migration rate was calculated as follows: Cell migration rate (%)=(initial wound area-wound area after 48 h)/initial wound area x100%.

Transwell assay. Cells were plated in 24-well Transwell chambers (Corning, Inc.), with the lower chambers containing 600 μl of complete medium. After 48 h, the cells in the upper chamber were removed using a cotton swab. The migrated or invaded cells were fixed with 4% paraformaldehyde at room temperature for 15 min, stained with 0.1% crystal violet for 30 min at room temperature and quantified manually using a Zeiss light microscope (Carl Zeiss AG).

RNA sequencing (RNA-seq). The RNA sequencing service was provided by CloudSeq Biotech Inc., which extracted RNA from cells using FreeZol reagent (Vazyme Biotech Co., Ltd.), with its quality and concentration evaluated using a NanoDrop-1000 spectrophotometer (Thermo Fisher Scientific, Inc.). rRNA was removed using an GenSeq® rRNA Removal Kit (GenSeq, Inc.) according to the manufacturer's instructions. RNA samples after rRNA removal were passed through the GenSeq® Low Input RNA Library Prep Kit (GenSeq, Inc.) to construct an RNA sequencing library. A BioAnalyzer 2100 instrument (Agilent Technologies, Inc.) was used for library quality control and quantification. 150 bp double-ended sequencing was performed on an Illumina NovaSeq instrument (Illumina, Inc.). Q30 (threshold for high-quality bases, with error rate <0.1%) was used for quality control. Cutadapt

software (24) (v1.9.3) was used to remove splices, subsequently low-quality reads were removed and high-quality reads were obtained. The filtered clean reads were then aligned to the reference genome with HISAT2 software (25) (v2.0.4). HTSeq software (26) (v0.9.1) was then used to generate the raw count and the edgeR (27) package was used to perform normalization and examine differentially expressed genes with a |log2 (fold change)| of ≥1 and false discovery rate of ≤0.05. Gene Ontology (GO) and pathway enrichment analysis were performed using the clusterProfiler package (27,28). Sequencing data have been uploaded to the National Center for Biotechnology Information (NCBI) Sequence Read Archive (SRA) (https://www.ncbi.nlm.nih.gov//bioproject/PRJNA1275425) under accession number (PRJNA1275425).

Tumor sphere formation assay. A549 cells were harvested and counted and 5,000 cells in serum-free DMEM-F12 (Gibco; Thermo Fisher Scientific, Inc.) containing EGF (20 ng/ml; PeproTech, Inc.), b-FGF (10 ng/ml; PeproTech, Inc.) and B27 (1:50 dilution, BD Biosciences) were plated in each well of six-well ultralow attachment plates (Corning, Inc.). After one week, the former tumor spheres were counted under a phase-contrast microscope (Carl Zeiss AG).

Immunofluorescence. A549 cells ($1x10^4$ cells/well) were grown on coverslips in 24-well plates at 37˚C for 24 h. Cells were fixed by 4% paraformaldehyde for 30 min, infiltrated with 0.2% Triton X-100 for 10 min, blocking with 5% bovine serum albumin (Beyotime Institute of Biotechnology) for 1 h at room temperature. Diluted CD133 antibodies (1:200 cat. no. 18470-1-AP; Proteintech Group, Inc.), ALDHA1 (1:200; cat. no. 83830-2-RR; Proteintech Group, Inc.), Vimentin (1:200; cat. no. 10366-1-AP; Proteintech Group, Inc.) and E-Cadherin (1:200; cat. no. 31863-1-AP; Proteintech Group, Inc.) antibodies were placed on glass slides and incubated overnight at 4˚C. Next, the coverslips were treated to Alexa Fluor 488 goat anti-rabbit IgG (1:200; cat. no. BA1127; Boster Biological Technology, Ltd.) or Alexa Fluor 594 goat anti-rabbit IgG (1:200; cat. no. BA1142; Boster Biological Technology, Ltd.) at room temperature for 1 h in the dark. Cells were washed and stained with 4',6-diamidino-2-phenylindole (DAPI, 1 mg/ml; 1:5,000; cat. no. S2110; Beijing Solarbio Science & Technology Co., Ltd.) for 10 min at room temperature. The images were imaged under a fluorescent microscope (Zeiss Axio Observer Z1 LSM710; Carl Zeiss AG).

Xenograft model and lung metastasis model. A total of 44 nude mice (female; aged 4-6 weeks; weight, 10-14 g) were acquired from the Comparative Medicine Center of Yangzhou University (Yangzhou, China; approval no.202406015) and raised in a specialized pathogen-free environment (21-26˚C; humidity, 40-70%; 12-h light/dark cycle and ad libitum access to food and water).

The mice were randomly divided into eight groups (4 groups for the xenograft models and 4 groups for the metastasis models). A suspension of $5x10^6$ A549 cells in 200 μl of PBS-Matrigel (1:1 ratio) was subcutaneously injected in the right underarm of mice. Mice were randomly divided (six mice/group) into four groups as follows: i) sh-NC group; ii) sh-NC+TGF-β1 group (sh-NC A549 cells pre-treated with 10 ng/ml TGF-β1 for 48 h before injection); iii) sh-Notch3 group; iv) sh-Notch3+TGF-β1 group (sh-Notch3 A549 cells pretreated with 10 ng/ml TGF-β1 for 48 h before injection). Tumor size was measured once a week with calipers and tumor volumes were calculated by the following formula: Volume (mm^3)=0.5 x Length (mm) x Width^2 (mm^2). Animals were checked daily and any animal found unexpectedly to be moribund, cachectic or unable to obtain food or water was sacrificed. In strict accordance with animal ethical regulations, the weight of tumors did not exceed 10% of the mouse body weight, the average tumor diameter did not exceed 20 mm, and the tumor volume did not exceed 2,000 mm^3. After 5 weeks, all animals were euthanized using a 30-70% per min displacement of chamber air with compressed CO_2. After the completion of euthanasia with CO_2 inhalation, cervical dislocation with the confirmation of a gap between the skull and spinal column was used to verify the death of mice. All tumors were dissected from mice and the total tumor weight in each mouse was measured. Some tumors were fixed in 4% formalin for 24 h at room temperature for subsequent immunohistochemistry. Additionally, the tumor metastasis model was created by injecting A549 cells into the tail veins of additional BALB/c nude mice. To perform this, $1x10^6$ cells mixed with PBS were injected into each mouse in 4 groups (n=5 per group). No metastatic nodules were found in the abdominal and thoracic organs of the subcutaneous xenograft mice. After 2 months, the mice were euthanized with excessive carbon dioxide and the lungs of the nude mice were extracted to observe whether there were metastatic lesions and stained with hematoxylin and eosin (H&E). After euthanasia, the death of the animals was confirmed based on the disappearance of pain response, no response when pressing the toes with hands or forceps and observation of cardiac and respiratory arrest. No nude mice experienced unexpected mortality during the experiment. All mice were euthanized at the planned end of the experiment.

Immunohistochemical (IHC) assay. The tumor tissues collected from a mouse xenograft model were fixed in 4% paraformaldehyde at 4˚C for 24 h and then embedded in paraffin. Sections of paraffin-embedded tissue (2-3 μm) were dried for 60 min at 60˚C and then subjected to two rounds of dewaxing in xylene for 30 min each. Subsequently, a decreasing gradient of alcohol concentrations was used for hydration. For antigen retrieval, the sections were heated in citrate buffer at 100˚C for 10 min. The sections were blocked with 5% BSA for 1 h at room temperature, and 3% H_2O_2 was used to block endogenous peroxidase/phosphatase activity for 10 min at room temperature. Subsequently, the sections were incubated overnight at 4˚C with the following primary antibodies: Anti-Vimentin (VIM) (1:5,000; cat. no. 10366-1-AP), anti-E-Cadherin antibody (1:500; cat. no. 31863-1-AP.), anti-CD44 antibody (1:500; cat. no. no. 60242-1-Ig) and anti-CD133 antibody (1:5,000; cat. no. 18470-1-AP) and anti-Ki67 (1:5,000; cat. no.27309-1-AP; all from Proteintech Group, Inc.). The sections were then treated with secondary antibodies labeled with biotin (1:1,000; cat. no. SA00001-2; Proteintech Group, Inc.) for 1 h at room temperature and incubated with an avidin solution labeled with horseradish peroxidase (HRP; Proteintech Group, Inc.) for 10 min at room temperature. The DAB staining solution

was incubated at room temperature for 15 min, and then hematoxylin was applied as the counterstain at room temperature for 3 min. Finally, the sections were dried by progressively adding ethanol, as well as xylene, and were subsequently sealed using neutral balsam. The results were observed using a light microscope.

H&E staining. The tissues were deparaffinized with xylene and immersed in an EDTA antigen retrieval buffer. Then, the tissues were stained with H&E. The sections were stained with hematoxylin dye for 2 min at room temperature, treated with 1% hydrochloric acid alcohol for 45 sec at room temperature, stained with eosin dye for 2 min at room temperature, dehydrated with ethanol (75, 85, 95 and 100%), washed with xylene and finally sealed with neutral resin. The results were observed under a light microscope.

Statistical analysis. The statistical analyses were performed using GraphPad 7.0 (GraphPad Software, Inc.; Dotmatics). Comparisons between two groups were performed using unpaired Student's t-test, while multi-group comparisons were analyzed using one-way ANOVA followed by Tukey's multiple comparison test. Data were expressed as means ± SD. $P<0.05$ was considered to indicate a statistically significant difference.

Results

Notch3 is upregulated in lung cancer and associated with poor prognosis. The present study first examined the expression of Notch3 in NSCLCs and bronchial epithelial cells (BEAS-2B). Western blotting and RT-qPCR showed that Notch3 protein and mRNA levels were highly expressed in the non-small cell lines and BEAS-2B (Fig. 1A and B). To evaluate the expression level of Notch3 in pathological tissues, the present study performed an expression analysis by comparing lung adenocarcinoma (LUAD) and lung squamous cell carcinoma (LUSC) to normal tissues by using the GEPIA server. It was found that Notch3 was clearly increased in NSCLC tissues (Fig. 1C). Meanwhile, the human protein atlas verified an obvious expression trend of Notch3 protein within NSCLC tissues (Fig. 1D).

Next, the relationship between Notch3 expression and prognosis in lung cancer patients was evaluated using the Kaplan-Meier plotter database. The results indicated that higher Notch3 expression was markedly associated with a poorer prognosis in lung cancer, with overall survival (OS) HR=1.3 [95% confidence interval (CI)=1.16-1.47; $P=1.4x10^{-5}$] and first progression (FP) HR=1.32 (95% CI=1.12-1.57; $P=1.1x10^{-3}$). However, Notch3 expression did not show a significant correlation with the prognosis of lung cancer patients in terms of post-progression survival (PPS; PPS HR=1.07, 95% CI=0.87-1.31, P=0.54) (Fig. 1E).

Transfection of Notch3 expressing vector and lentivirus into lung cancer cells. Notch3 intracellular domain (N3ICD) overexpression plasmid was transfected into A549 and H1975 cells and its expression was confirmed by WB. Compared with the empty vector-transfected cells, the protein levels of N3ICD were markedly increased in the plasmid-transfected cells (Fig. 2A). Lentivirus was employed to establish stable cell lines with downregulated (shNotch3) expression levels of Notch3 in A549 cells. Among the three virus sequences, the silencing efficiency of Notch3 was assessed using RT-qPCR and WB (Fig. 2C and D) and selected the sequence with the highest silencing efficiency for further experiments. When N3ICD was upregulated in lung cancer cells, CCK-8 assay results showed that the viability of lung cells was enhanced, whereas Notch3 knockdown resulted in decreased cell viability (Fig. 2B and E).

Notch3 induced EMT via TGF-β1 production. The present study then compared the transcriptomes between A549 cells with control (shNC) and Notch3 knockdown (shNotch3) by RNA sequencing. KEGG analysis revealed that the TGF-β signaling pathway was markedly affected by Notch3 knockdown (Fig. 3A). Volcano plots, generated using P-values and fold changes, helped visualize the differential gene expression between the control and sh-Notch3 groups. The RNA sequencing results showed that 345 genes were upregulated, while 321 were downregulated (Fig. 3B). Additionally, hierarchical clustering revealed distinct differences between the control and sh-Notch3 groups (Fig. 3C). Moreover, by constructing PPI networks, associations between Notch3 and TGF-β1 were identified, as well as with EMT-associated proteins such as VIM and CDH1 (Fig. 3D). The GEPIA server was used to analyze the correlation between Notch3 and TGF-β1 in normal lung tissues and lung cancer, as well as EMT-related markers. TGF-β1 and VIM were markedly positively associated with Notch3, while E-Cadherin (CDH1) showed a negative correlation (Fig. 3E). These findings suggested a strong association between Notch3 and EMT markers.

Given that TGF-β1-induced EMT is well-established in cell lines such as H1975, H1299 and A549, the role of Notch3 in this process was further investigated. To confirm this, overexpressed N3ICD plasmids and Notch3-knockdown lentiviruses were transfected into A549 and H1975 cells. The results showed that TGF-β1 secretion increased upon N3ICD overexpression, while TGF-β1 secretion decreased after Notch3 knockdown (Fig. 3F). This suggests that Notch3 may promote EMT by upregulating TGF-β production. Western blotting further confirmed the relationship between Notch3 and EMT markers in both cell types. After transfecting the N3ICD overexpression plasmid and Notch3-silencing siRNA into A549 and H1975 cells and treating them with TGF-β1 (Fig. 3G), N3ICD overexpression enhanced TGF-β1-induced changes in EMT marker expression, resulting in a marked increase in VIM levels and a reduction in E-Cadherin expression. By contrast, silencing Notch3 reversed these TGF-β1-mediated changes in EMT marker expression.

Notch3 mediates TGF-β1-induced proliferation, migration and invasion of lung cancer cells. The present study investigated the role of Notch3 in TGF-β1-induced EMT in lung cancer by silencing or overexpressing N3ICD in lung cancer cells. The results showed that increased Notch3 expression in A549 and H1975 cells markedly enhanced cell proliferation, while reduced Notch3 levels inhibited cell proliferation. Notably, TGF-β1 itself did not have a significant effect on cell proliferation (Fig. 4A). Transwell and wound healing assays revealed that Notch3 knockdown reversed the inhibitory effect of TGF-β1 on cell migration and invasion, whereas

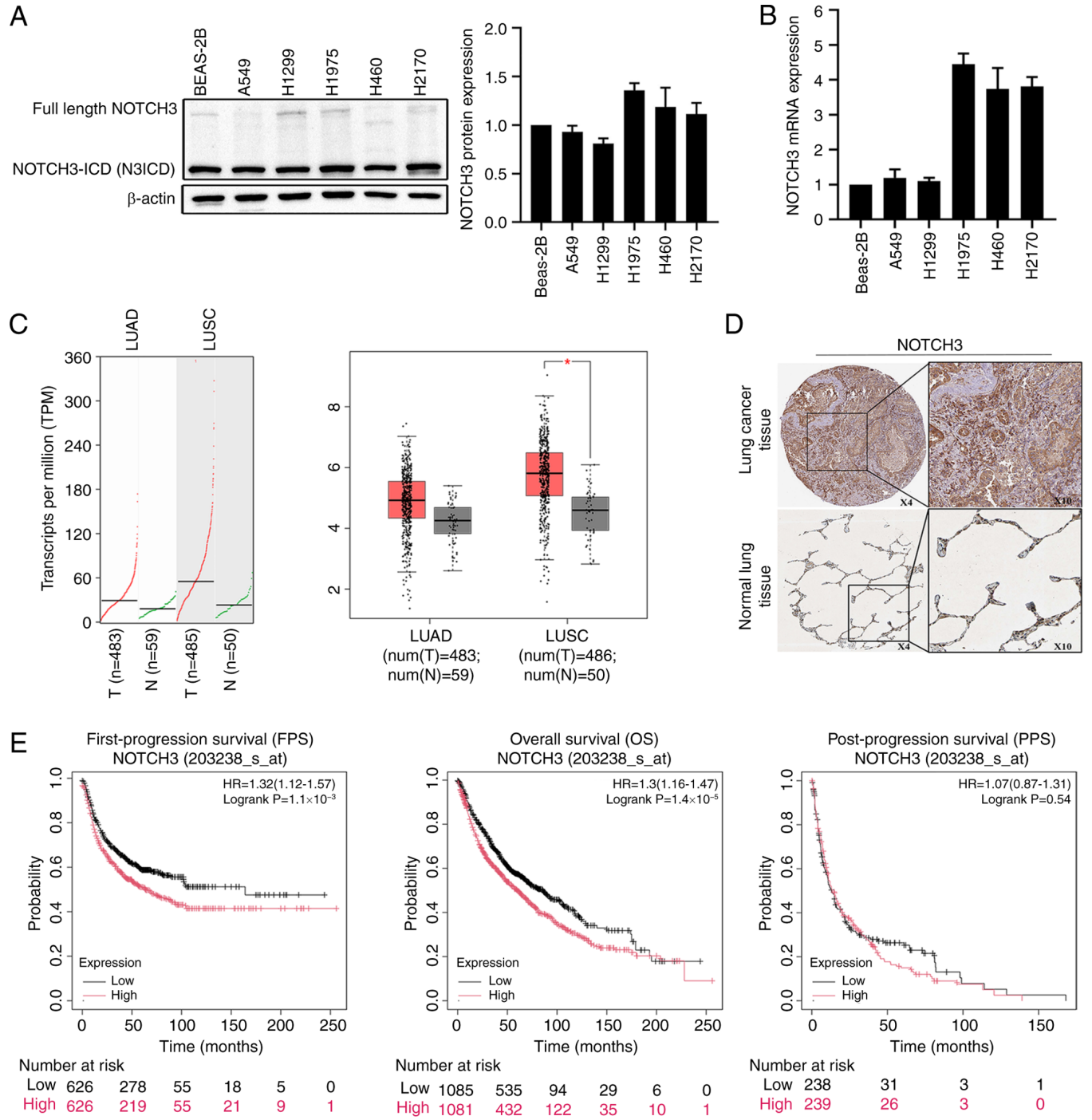

Figure 1. Notch3 expression in the lung cancer and related to unfavorable prognosis in NSCLC patients. (A) Expression of Notch3 protein in the indicated cell lines was determined by western blotting. (B) Relative Notch3 gene expression was examined in the indicated cell lines. (C) Differential expression of Notch3 between tumor (n=979) and adjacent normal (n=685) tissues in NSCLC. (D) Notch3 protein expression in normal lung tissue and NSCLC specimens. Images were obtained from the Human Protein Atlas online database. (E) Correlation between Notch3 and prognosis of lung cancer in the Kaplan-Meier plotter database. NSCLC, non-small cell lung cancer; HR, hazard ratio.

N3ICD overexpression had the opposite effect, promoting cell migration and invasion in lung cancer cells (Fig. 4B and C). In conclusion, these results suggest that Notch3 promotes EMT by activating TGF-β1.

Enrichment and identification of CSCs from A549 cells. One of the effective acquisition methods for CSCs is SFM suspension culture. Based on the experimental requirements, the human lung cell line A549 was cultured in SFM culture conditions to enrich related CSCs. After three passages in culture, numerous spheroid clusters were observed using microscopy (Fig. 5A). CD133 and ALDH1A are two of the most well characterized biomarkers of lung cancer (29). Immunofluorescence staining showed that sphere cells exhibited a higher expression of CD133 and ALDH1A Compared with parental cells (Fig. 5B). To further investigate the difference in cancer stemness between parental and sphere cells, the cells were collected and the expression of stem cell transcription factors and stem

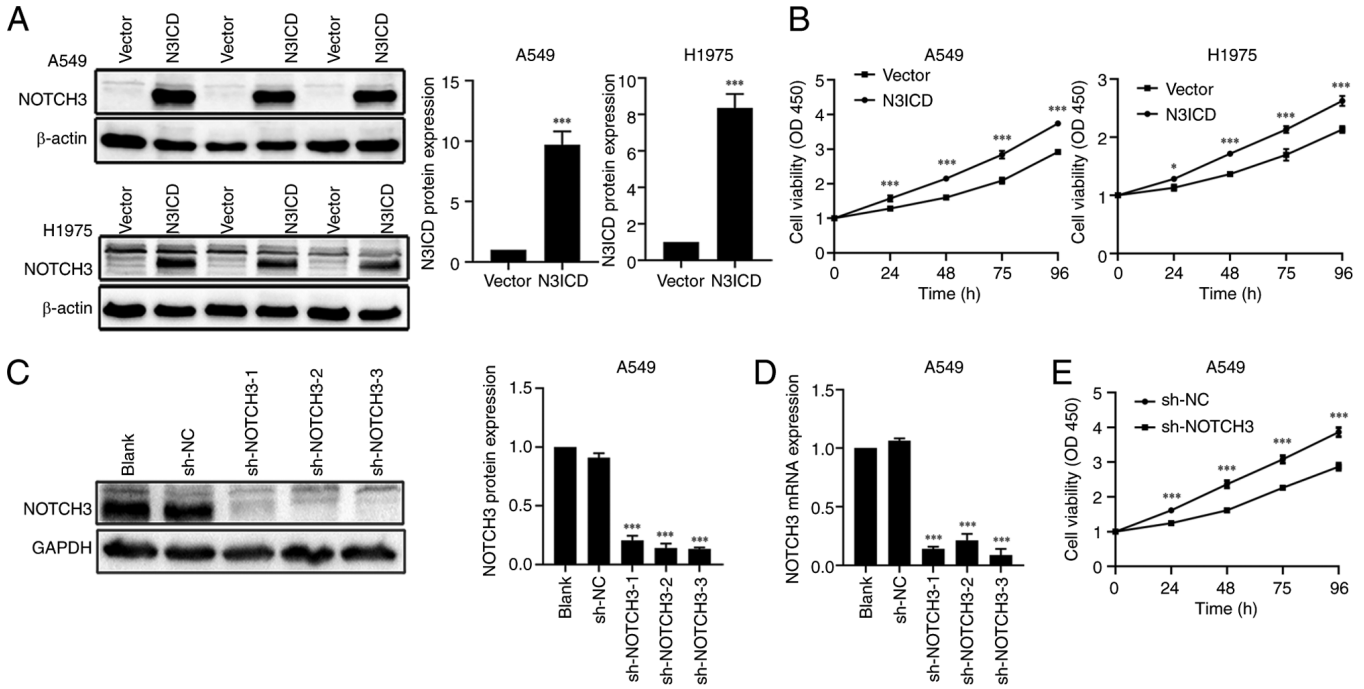

Figure 2. A549 and H1975 cells were transfected with Notch3-expressing or empty vector and A549 cells were transfected with Notch3 knock-down lentivirus. (A) A549 and H1975 cells were transfected with Notch3 expressing or empty vector, at 48 h after transfection, protein expression of Notch3 were analyzed by WB. (B) Cell viability was measured after CCK-8 staining. (C) WB and (D) RT-qPCR validate the efficiency of constructed Notch3 knockdown A549 cells. (E) Cell viability was measured after CCK-8 staining. Data are presented as mean ± SD. *P<0.05 and ***P<0.001. WB, western blotting; CCK-8, Cell Counting Kit-8; RT-qPCR, reverse transcription quantitative polymerase chain reaction; sh, short hairpin; NC, negative control.

cell markers assessed. Sphere cells showed markedly higher expression levels of Oct4, Sox4, CD133 and Nanog Compared with parental cells (Fig. 5C). Additionally, WB of stem cell markers confirmed that sphere cells exhibited elevated levels of CD133, CD44, OCT4 and ALDH1A Compared with parental cells (Fig. 5D). Enhanced tumor invasion, a hallmark of CSCs, was observed in the Transwell assay (Fig. 5E). Taken together, these results indicated that the sphere cells derived from A549 cells were successfully enriched and exhibited CSC characteristics, making them suitable for further experimentation.

Expression pattern of CSCs derived from NSCLCs. Activation of the EMT is an important process for the transformation of common tumor cells into CSCs, which in turn promotes the formation of CD133+/ALDH1+ subpopulations. EMT is also closely linked to tumor progression, metastasis and drug resistance. It was observed that the expression of the epithelial marker E-Cadherin was markedly downregulated in A549 spheres Compared with parental cells, while the mesenchymal marker VIM was markedly upregulated (Fig. 6A-C). Furthermore, TGF-β1 secretion was notably increased in A549 spheres Compared with parental cells (Fig. 6D). These findings suggested that the formation of cancer stemness may be accompanied by the activation of EMT. The expression of Notch3 was next examined using WB. The results showed that Notch3 expression was elevated in A549 spheres (Fig. 6E). Based on these observations, it was concluded that Notch3 is associated with A549-derived CSCs.

Notch3 drives cancer stemness via TGF-β1 in lung cancer. The present study investigated the role of Notch3 in regulating self-renewal by assessing the sphere formation ability. It was found that Notch3 knockdown led to a decrease in spheroid formation in A549 cells after TGF-β1 stimulation, Compared with control cells. By contrast, N3ICD overexpression resulted in an increased number of spheroids following TGF-β1 stimulation (Fig. 7A). Additionally, WB showed that overexpression of Notch3 markedly enhanced the TGF-β1-induced upregulation of stemness markers. However, inhibition of Notch3 expression markedly reduced the TGF-β1-induced increase in stemness marker expression (Fig. 7B). These results strongly suggest that Notch3 positively regulates the stemness of lung cancer cells through TGF-β1.

Downregulation of Notch3 inhibits TGF-β1-driven tumor growth and lung metastasis in nude mice. To confirm whether Notch3 expression could inhibit the tumorigenesis of lung cells *in vivo*, A549 cells infected with a specific shRNA targeting Notch3 or a mock shRNA control were implanted into BALB/c nude mice and TGF-β1 was injected intraperitoneally as described in the Materials and methods section. The tumor volume was examined every 7 days. Compared with the control group, the TGF-β1 group demonstrated an increase in tumor volume, whereas a decreased tumor volume was observed in the Sh-Notch3 group. After 35 days, the xenografts were exercised from the mice and similar changes in tumor volume and weight were observed. These findings suggested that Notch3 antagonized TGF-β1-induced tumor growth (Fig. 8A).

The protein expression levels of E-Cadherin, VIM, CD133, CD44 and Ki-67 in the transplanted tumor tissues were assessed using immunohistochemistry. Sh-Notch3 reduced the protein levels of VIM, Ki-67, CD44 and CD133 and

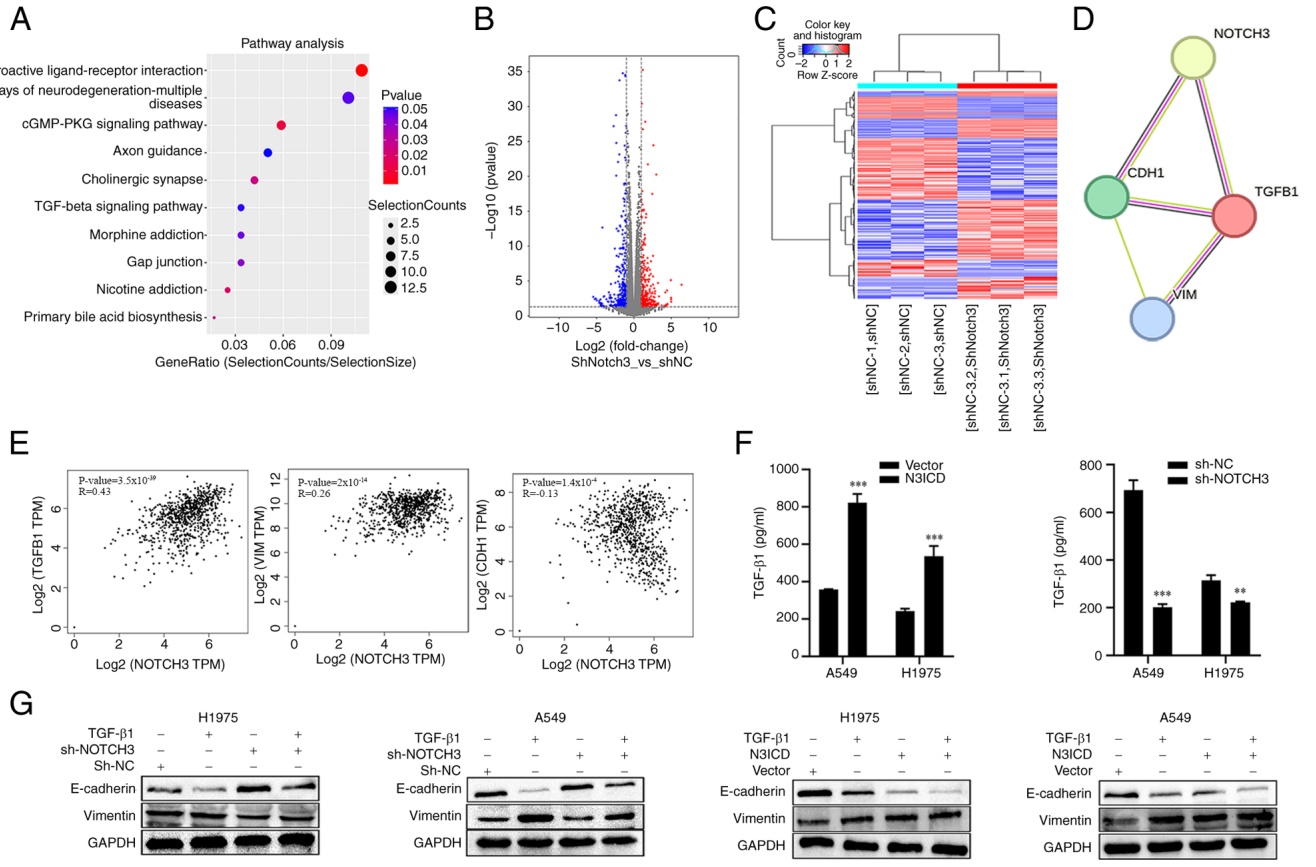

Figure 3. Notch3 drives the EMT through TGF-β1 signaling. (A) Gene Ontology analysis of differentially expressed genes after Notch3 knockdown. (B) Volcano plots of differentially expressed genes. Red dots and blue dots represent up- and downregulated genes, respectively. (C) Heat map of the indicated target genes in Notch3-silenced and control cells. The target genes of TGF-β1 signaling were decreased in Notch3-silenced cells. (D) Using the STRING program to analyses the Notch3, TGF-β1, Vimentin and E-Cadherin (CDH1). (E) Bioinformatic analysis revealed a correlation between Notch3 and TGF-β1 and EMT-related genes (E-Cadherin and Vimentin) expression. (F) Transfection of H1975 and A549 cells with Notch3 vector or Notch3 shRNA. After transfection, TGF-β1 production in the culture supernatant was measured using an ELISA. (G) Notch3 was either overexpressed or silenced in H1975 and A549 cell lines, followed by treatment with or without 10 ng/ml TGF-β1 48 h. EMT markers E-Cadherin and Vimentin were analyzed by WB. Data are presented as mean ± SD. **P<0.01 and ***P<0. 001. EMT, epithelial-mesenchymal transition; TGF-β1, transforming growth factor-β; sh, short hairpin; NC, negative control; ELISA, enzyme-linked immunosorbent assay; WB, western blotting.

increased E-Cadherin expression. By contrast, the TGF-β1 group exhibited the opposite effects. Notably, sh-Notch3 reversed the inhibitory effect of TGF-β1 on E-Cadherin expression and attenuated the TGF-β1-induced upregulation of VIM, CD44, CD133 and Ki-67 (Fig. 8B). Next, a metastatic model was established by injecting A549 cells via the tail vein of the mice, followed by intraperitoneal TGF-β1 injection. Compared with the negative control group, the Notch3 knockdown group exhibited a decrease in the number of lung metastatic nodules, while TGF-β1 induction markedly increased the number of metastatic nodules. Interestingly, Notch3 knockdown decreased the number of TGF-β1-induced lung metastatic nodules (Fig. 8C). These results confirm that Notch3 knockdown inhibits TGF-β1-induced tumorigenesis and metastasis of A549 cells *in vivo*.

Discussion

Lung cancer is a common malignant tumor characterized by rapid growth, high metastasis rate and poor prognosis (30). The Notch signaling pathway is an evolutionarily conserved intercellular communication mechanism that plays a key role in both lung development and disease. Among the Notch family, Notch1 and Notch3 are particularly important (16,31). Overactivation of the Notch1/3 signaling pathway is associated with the initiation and progression of lung cancer (22,31,32). Multiple studies emphasized that Notch3 is an oncogene in NSCLC and inhibiting Notch3 can suppress cell proliferation (22,33,34). The present study confirmed that Notch3 is highly expressed in NSCLC and is linked to poor prognosis in patients. However, the precise molecular mechanisms by which Notch3 influences the onset and development of NSCLC remain poorly understood.

EMT refers to the process by which epithelial cells transform into mesenchymal cells under certain physiological or pathological conditions (35). The growth factor TGF-β in the tumor microenvironment has garnered attention for its role in initiating EMT (36). In lung cancer, it has been reported that TGF-β promotes EMT in the lung adenocarcinoma cell lines by enhancing the Smad signaling pathway (37). Additionally, studies have shown that TGF-β can regulate the EMT process to block the growth and progression of liver cancer and this effect is markedly diminished when TGF-β signaling is inhibited (38-41). The present study further confirmed that lung

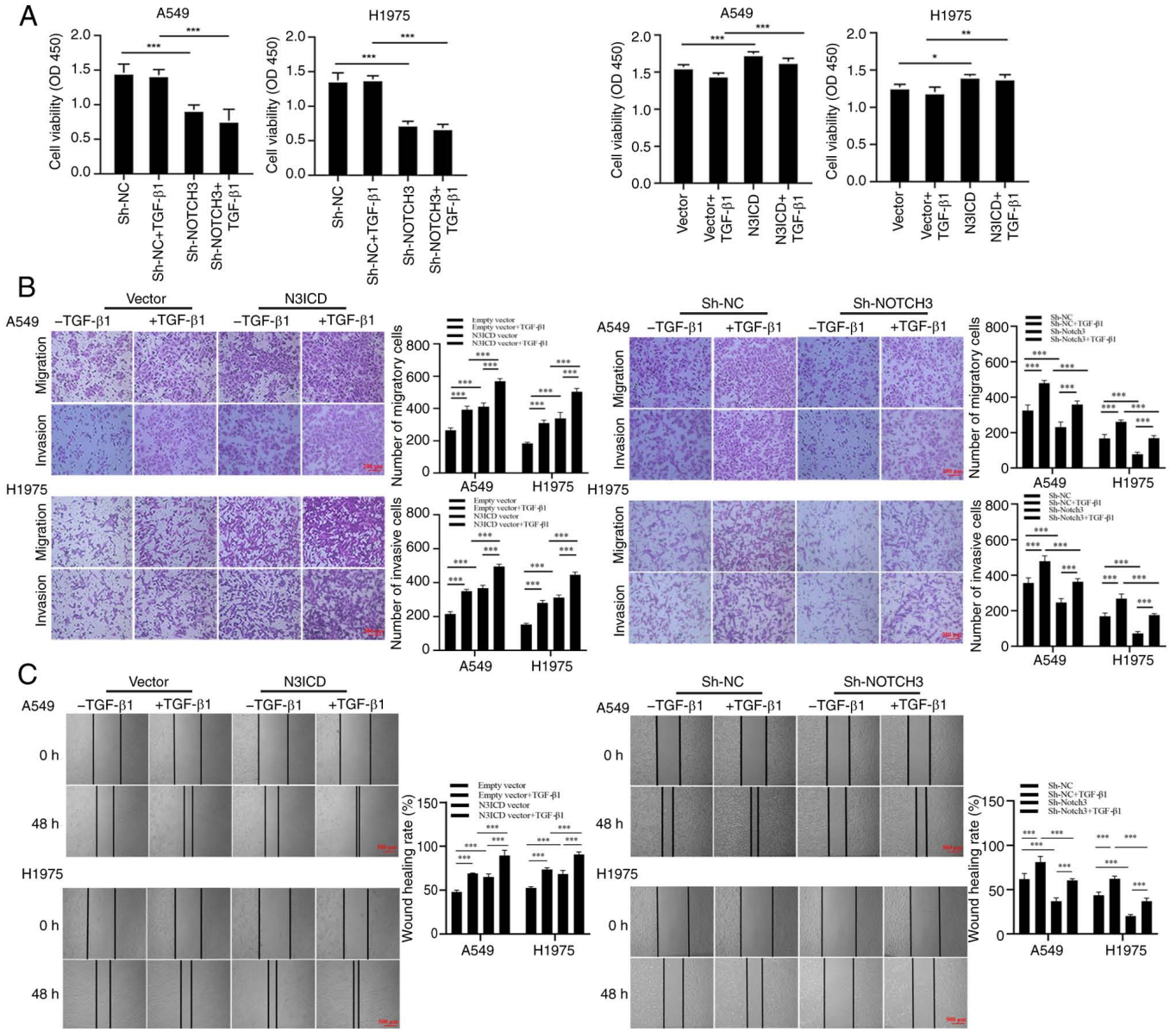

Figure 4. Notch3 mediates TGF-β1 induced proliferation, migration and invasion of H1975 and A549 cell lines. Notch3 was either overexpressed or silenced in H1975 and A549 cell lines, followed by treatment with or without 10 ng/ml TGF-β1 48 h. (A) Cell proliferation was detected by the CCK-8 detection kit. (B) Cell migration invasion assay using Transwell. Scale bar, 200 μm. (C) A wound healing assay. Scale bar, 500 μm. Data are presented as mean ± SD. *P<0.05, **P<0.01 and ***P<0.001. TGF-β1, transforming growth factor-β; CCK-8, Cell Counting Kit-8.

cancer cells exhibited EMT characteristics upon stimulation with various concentrations and time points of TGF-β1.

Notch3 signaling has different roles in lung cancer cell lines. In small cell lung cancer (SCLC), Notch3 expression is associated with the inhibition of EMT and cell motility. By contrast, in NSCLC, inhibiting Notch3 leads to a reduction in cell proliferation, EMT and motility (22). Studies suggest that the TGF-β and Notch3 signaling pathways frequently cross-regulate EMT, with Notch3 enhancing TGF-β-induced EMT (42). TGF-β activates Notch signaling by upregulating the expression of Notch ligands and receptors, including Jagged1, which binds to Notch receptors to activate downstream targets (43). However, the activation of Notch3 can enhance the transcriptional activity of EMT-related factors such as ZEB1, thereby promoting the EMT phenotype and facilitating metastasis (42,44). Consequently, these two pathways (TGF-β and Notch3) collaborate to mediate EMT and cancer progression, with Notch3 potentially amplifying the effects of TGF-β on cellular plasticity and invasiveness (42,45). The present study further validated through *in vivo* and *in vitro* experiments that knockdown of Notch3 inhibited TGF-β1-induced migration, invasion and EMT in NSCLC. On the other hand, overexpression of N3ICD promoted TGF-β1-induced EMT in NSCLC cells, suggesting that N3ICD may play a crucial role in tumor promotion, particularly in NSCLC EMT.

EMT not only enhances the migratory and invasive abilities of tumor cells but also induces cancer cells to acquire stem cell-like characteristics (8). These stem cell-like traits include self-renewal, resistance to conventional treatments and the ability to initiate tumor formation. During EMT, cancer cells gain the capacity for self-renewal, resist apoptosis and exhibit pluripotency, all of which are hallmarks of

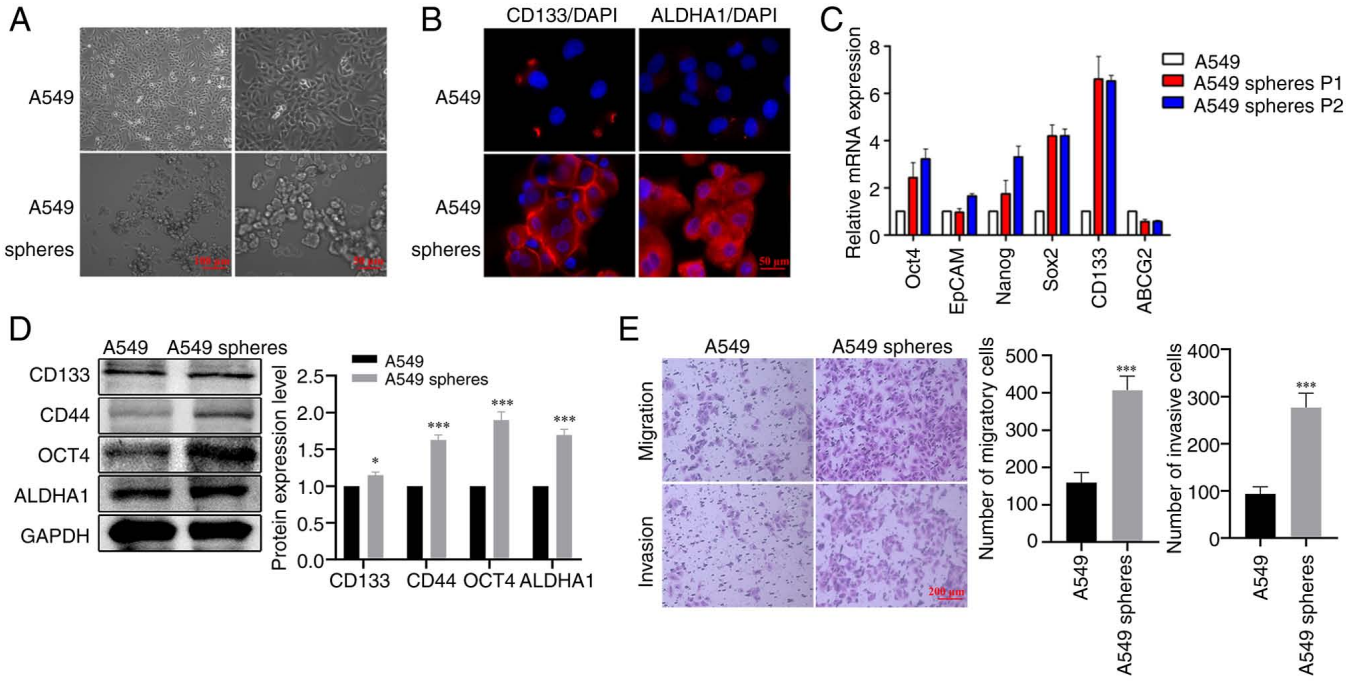

Figure 5. Spherical cells derived from lung cancer cells exhibit cancer stem cell characteristics. (A) The morphologies of adherent A549 cells and A549 cell spheres. Scale bar, 100 μm (left) and 50 μm (right). (B) Immunofluorescence of the stemness markers in A549 spheres. The nuclei were stained with DAPI. Scale bar, 50 μm. (C) The mRNA expression levels of stem cell markers in A549 and A549 spheres. (D) Western blotting of stemness markers (OCT4, CD44, CD133 and ALDHA1) in A549 and A549 spheres. (E) Transwell migration invasion assay of parental cells and sphere cells. Scale bar, 200 μm. Data are presented as mean ± SD. *P<0.05 and ***P<0.001.

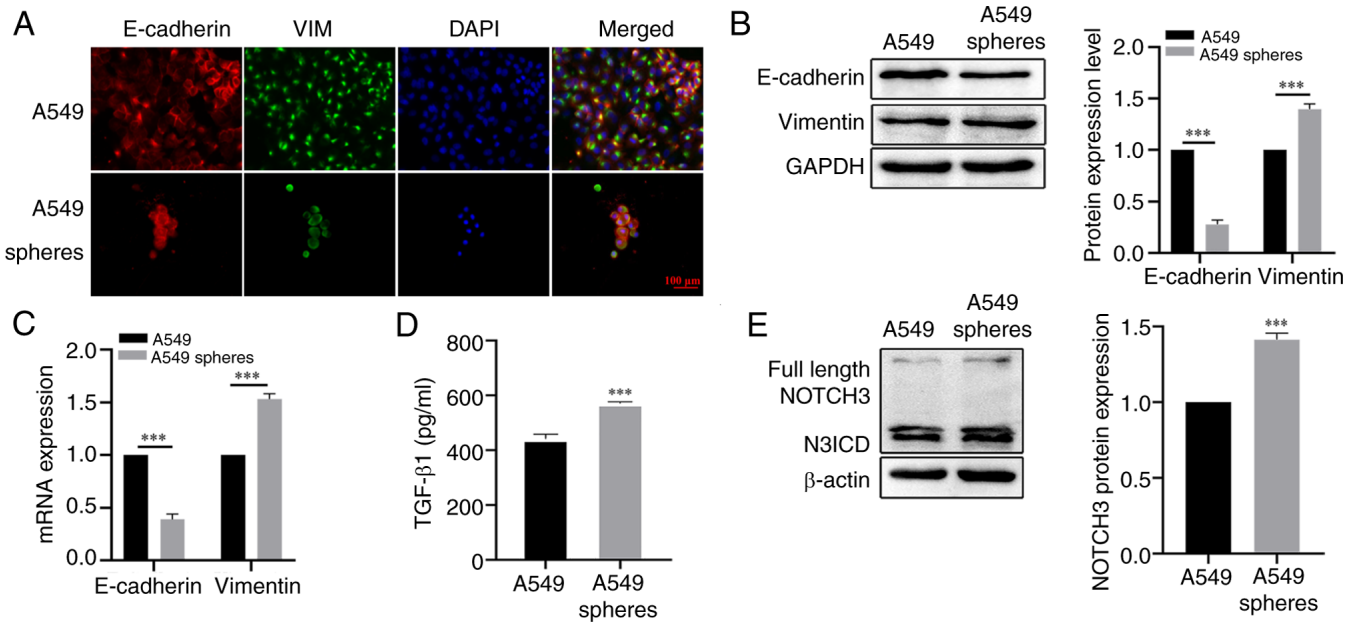

Figure 6. Molecular properties of A549 CSCs. (A) Immunofluorescence staining for E-Cadherin and Vimentin expression in A549 cells and A549-spheres. Scale bar, 100 μm. (B) WB and (C) RT-qPCR show E-Cadherin and Vimentin expressions in A549 cells and A549 CSCs. (D) TGF-β1 production in the culture supernatant was measured using an ELISA. (E) Western blotting shows Notch3 expression in A549 cells and A549 CSCs. Data are presented as mean ± SD. ***P<0.001. CSCs, cancer stem cells; RT-qPCR, reverse transcription quantitative polymerase chain reaction; ELISA, enzyme-linked immunosorbent assay.

CSCs (11,33,46). In addition to its role in EMT, Notch3 has been shown to directly regulate genes involved in stemness and proliferation, such as OCT4, SOX2 and Nanog (47,48). This makes Notch3 a crucial regulator in cancer stem cell populations. The present study further confirmed that silencing Notch3 reduced the ability of TGF-β to inhibit tumor sphere formation, impaired the ability of lung cancer cells to initiate tumors and decreased the expression of stemness markers at the protein level. By contrast, overexpression of N3ICD contributes to maintaining the tumorigenicity of lung CSCs. Therefore, targeting the Notch3 signaling pathway could provide strategies to reverse EMT, reduce the

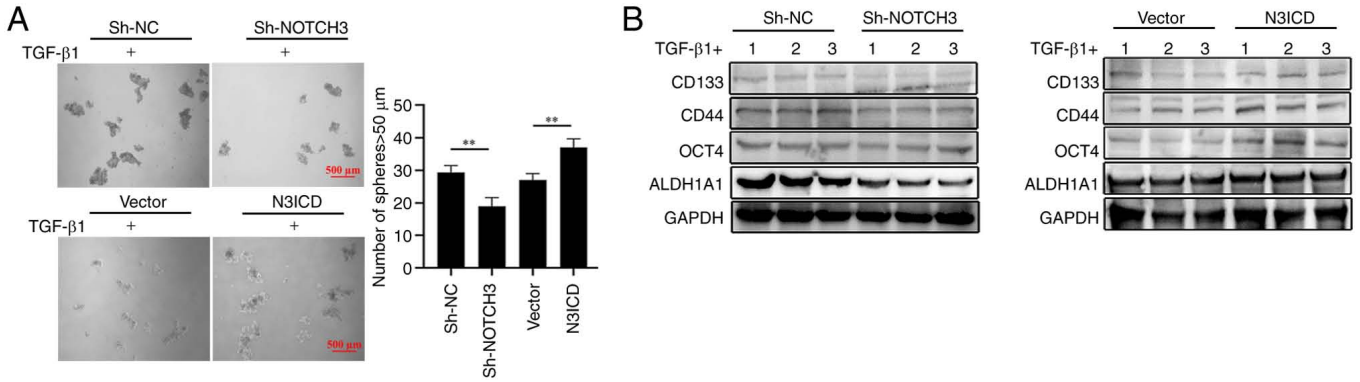

Figure 7. Notch3 promotes the stemness of A549 CSCs via TGF-β1. (A) Sphere-formation ability was detected in A549 CSCs with Notch3 overexpression or knockdown after 10 ng/ml TGF-β1 stimulation. Scale bar, 500 μm (B) The expression of stemness markers (OCT4, CD44, CD133 and ALDHA1) was examined in A549 CSCs with Notch3 overexpression or knockdown after TGF-β1 stimulation. Data are presented as mean ± SD. **P<0.01. CSCs, cancer stem cell stemness; TGF-β1, transforming growth factor-β; sh, short hairpin; NC, negative control.

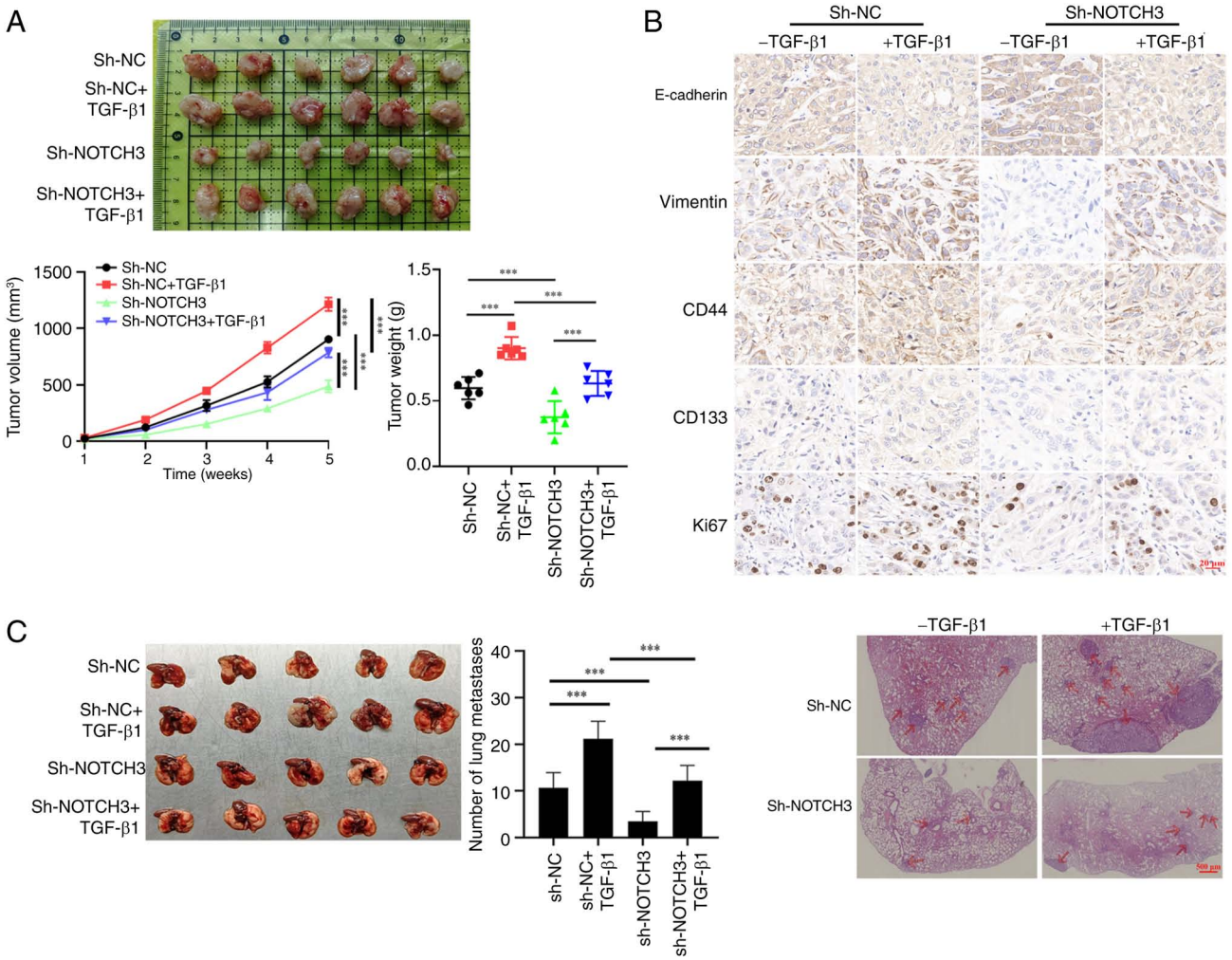

Figure 8. Notch3 promotes TGF-β1-driven tumorigenicity and the metastasis of lung cancer in nude mice. (A) Xenograft tumor volume and weight of the xenograft tumors were measured after mice were sacrificed, Notch3 knockdown suppressed tumor growth (n=6 per group). (B) Immunohistochemistry analysis of E-Cadherin, Vimentin, CD44, CD133 and Ki67 expression in tumor tissues. Scale bar, 20 μm. (C) Notch3 knockdown reduced the numbers of metastatic nodules stained with hematoxylin-eosin. Scale bar, 500 μm. Data are presented as mean ± SD. ***P<0.001. TGF-β1, transforming growth factor-β; sh, short hairpin; NC, negative control.

CSC population and overcome treatment resistance, offering potential clinical benefits in the treatment of metastatic and chemotherapy-resistant cancers.

For the *in vivo* experiments, female mice were selected due to several key factors. They generally exhibit lower aggression and territorial behaviors compared with males, which

helps minimize stress-related variability and confounding factors (49). Moreover, female mice consistently show higher tumor take rates in lung cancer xenografts and maintain more stable hormonal profiles, as the absence of estrus cycle synchronization avoids the fluctuations in male testosterone levels that could potentially affect tumor growth dynamics (50,51). Future studies could compare both sexes to explore potential sex-specific effects of Notch3 modulation in lung cancer progression.

It is worth noting that while both A549 and H1975 cell lines were included in the initial EMT studies, only A549 cells were used for subsequent tumor sphere formation and stemness assays. This decision was made due to time constraints and limited experimental resources. Importantly, A549 and H1975 are both adenocarcinoma-derived NSCLC cell lines and the EMT-related experiments revealed similar responses to TGF-β1 treatment in both lines. Therefore, A549 was selected as a representative model for stemness studies. The authors acknowledge the importance of validating these findings in additional cell lines such as H1975 and this will be addressed in future studies. This limitation will also be clarified in the revised manuscript to ensure transparency.

In summary, the present study underscored the pivotal role of Notch3 in driving CSCs and EMT through TGF-β1, which contribute to the aggressiveness and metastatic potential of lung cancer. These findings offer valuable insights into the molecular mechanisms underlying cancer progression and underscore the potential of both Notch3 and TGF-β1 as promising therapeutic targets in NSCLC. Further research is warranted to explore the clinical implications and therapeutic opportunities associated with targeting Notch3 and TGF-β1 in these malignancies.

Acknowledgements

Not applicable.

Funding

The present study was partly supported by the National Natural Science Foundation of China (grant no. 81800049) and The Research Fund of North Jiangsu People's Hospital (grant no. SBLC22002).

Availability of data and materials

The RNA sequencing data generated in the present study may be found in the Sequence Read Archive (SRA) database under accession number PRJNA1275425 or at the following URL: https://www.ncbi.nlm.nih.gov//bioproject/PRJNA1275425. All other data generated in the present study may be requested from the corresponding author.

Authors' contributions

QG designed the study. writing and/or revising the manuscript was conducted by FW and SH. Edited and reviewed by XX and JY. JY and LC confirm the authenticity of all the raw data. LC, LS, QG and JB analyzed data. All authors read and approved of the final manuscript.

Ethics approval and consent to participate

The whole procedure was performed according to the Guide for the Care and Use of Laboratory Animals (The Ministry of Science and Technology of China, 2006) and The Regulation on the Administration of Laboratory Animals (State Council Decree No. 676, 2017; URL: http://www.most.gov.cn/). All animal experiments were approved by Experimental Animal Welfare Ethics Committee of Comparative Medical Center of Yangzhou University (approval no. 202406015).

Patient consent for publication

Not applicable.

Competing interests

The authors declare that they have no competing interests.

References

1. Altorki NK, Markowitz GJ, Gao D, Port JL, Saxena A, Stiles B, McGraw T and Mittal V: The lung microenvironment: An important regulator of tumour growth and metastasis. Nat Rev Cancer 19: 9-31, 2019.
2. Zaman A and Bivona TG: Emerging application of genomics-guided therapeutics in personalized lung cancer treatment. Ann Transl Med 6: 160, 2018.
3. Gregg JP, Li T and Yoneda KY: Molecular testing strategies in non-small cell lung cancer: Optimizing the diagnostic journey. Transl Lung Cancer Res 8: 286-301, 2019.
4. Khan AQ, Hasan A, Mir SS, Rashid K, Uddin S and Steinhoff M: Exploiting transcription factors to target EMT and cancer stem cells for tumor modulation and therapy. Semin Cancer Biol 100: 1-16, 2024.
5. Tsai JH and Yang J: Epithelial-mesenchymal plasticity in carcinoma metastasis. Genes Dev 27: 2192-2206, 2013.
6. Thiery JP, Acloque H, Huang RY and Nieto MA: Epithelial-mesenchymal transitions in development and disease. Cell 139: 871-890, 2009.
7. Zavadil J and Böttinger EP: TGF-beta and epithelial-to-mesenchymal transitions. Oncogene 24: 5764-5774, 2005.
8. Babaei G, Aziz SG and Jaghi NZZ: EMT, cancer stem cells and autophagy; The three main axes of metastasis. Biomed Pharmacother 133: 110909, 2021.
9. Zhang C, Ding XP, Zhao QN, Yang XJ, An SM, Wang H, Xu L, Zhu L and Chen HZ: Role of α7-nicotinic acetylcholine receptor in nicotine-induced invasion and epithelial-to-mesenchymal transition in human non-small cell lung cancer cells. Oncotarget 7: 59199-59208, 2016.
10. Han J, Won M, Kim JH, Jung E, Min K, Jangili P and Kim JS: Cancer stem cell-targeted bio-imaging and chemotherapeutic perspective. Chem Soc Rev 49: 7856-7878, 2020.
11. Lytle NK, Barber AG and Reya T: Stem cell fate in cancer growth, progression and therapy resistance. Nat Rev Cancer 18: 669-680, 2018.
12. Singh SK, Hawkins C, Clarke ID, Squire JA, Bayani J, Hide T, Henkelman RM, Cusimano MD and Dirks PB: Identification of human brain tumour initiating cells. Nature 432: 396-401, 2004.
13. Mani SA, Guo W, Liao MJ, Eaton EN, Ayyanan A, Zhou AY, Brooks M, Reinhard F, Zhang CC, Shipitsin M, *et al*: The epithelial-mesenchymal transition generates cells with properties of stem cells. Cell 133: 704-715, 2008.
14. Kovall RA, Gebelein B, Sprinzak D and Kopan R: The canonical notch signaling pathway: Structural and biochemical insights into shape, sugar, and force. Dev Cell 41: 228-241, 2017.
15. Luca VC, Kim BC, Ge C, Kakuda S, Wu D, Roein-Peikar M, Haltiwanger RS, Zhu C, Ha T and Garcia KC: Notch-Jagged complex structure implicates a catch bond in tuning ligand sensitivity. Science 355: 1320-1324, 2017.
16. Sun J, Dong M, Xiang X, Zhang S and Wen D: Notch signaling and targeted therapy in non-small cell lung cancer. Cancer Lett 585: 216647, 2024.

17. Zheng Y, de la Cruz CC, Sayles LC, Alleyne-Chin C, Vaka D, Knaak TD, Bigos M, Xu Y, Hoang CD, Shrager JB, *et al*: A rare population of CD24(+)ITGB4(+)Notch(hi) cells drives tumor propagation in NSCLC and requires Notch3 for self-renewal. Cancer Cell 24: 59-74, 2013.
18. Konishi J, Kawaguchi KS, Vo H, Haruki N, Gonzalez A, Carbone DP and Dang TP: Gamma-secretase inhibitor prevents Notch3 activation and reduces proliferation in human lung cancers. Cancer Res 67: 8051-8057, 2007.
19. Ma Y, Li M, Si J, Xiong Y, Lu F, Zhang J, Zhang L, Zhang P and Yang Y: Blockade of Notch3 inhibits the stem-like property and is associated with ALDH1A1 and CD44 via autophagy in non-small lung cancer. Int J Oncol 48: 2349-2358, 2016.
20. Ye YZ, Zhang ZH, Fan XY, Xu XL, Chen ML, Chang BW and Zhang YB: Notch3 overexpression associates with poor prognosis in human non-small-cell lung cancer. Med Oncol 30: 595, 2013.
21. Yuan X, Wu H, Xu H, Han N, Chu Q, Yu S, Chen Y and Wu K: Meta-analysis reveals the correlation of Notch signaling with non-small cell lung cancer progression and prognosis. Sci Rep 5: 10338, 2015.
22. Hassan WA, Yoshida R, Kudoh S, Motooka Y and Ito T: Evaluation of role of Notch3 signaling pathway in human lung cancer cells. J Cancer Res Clin Oncol 142: 981-993, 2016.
23. Livak KJ and Schmittgen TD: Analysis of relative gene expression data using real-time quantitative PCR and the 2(-Delta Delta C(T)) method. Methods 25: 402-408, 2001.
24. Martin M: Cutadapt removes adapter sequences from high-throughput sequencing reads. EMBnet J 17: 10-12, 2011.
25. Kim D, Langmead B and Salzberg SL: HISAT: A fast spliced aligner with low memory requirements. Nat Methods 12: 357-360, 2015.
26. Anders S, Pyl PT and Huber W: HTSeq-a Python framework to work with high-throughput sequencing data. Bioinformatics 31: 166-169, 2015.
27. Robinson MD, McCarthy DJ and Smyth GK: edgeR: A bioconductor package for differential expression analysis of digital gene expression data. Bioinformatics 26: 139-140, 2010.
28. Yu G, Wang LG, Han Y and He QY: clusterProfiler: An R package for comparing biological themes among gene clusters. OMICS 16: 284-287, 2012.
29. Eramo A, Lotti F, Sette G, Pilozzi E, Biffoni M, Di Virgilio A, Conticello C, Ruco L, Peschle C and De Maria R: Identification and expansion of the tumorigenic lung cancer stem cell population. Cell Death Differ 15: 504-514, 2008.
30. Leiter A, Veluswamy RR and Wisnivesky JP: The global burden of lung cancer: Current status and future trends. Nat Rev Clin Oncol 20: 624-639, 2023.
31. Zong D, Ouyang R, Li J, Chen Y and Chen P: Notch signaling in lung diseases: Focus on Notch1 and Notch3. Ther Adv Respir Dis 10: 468-484, 2016.
32. Wael H, Yoshida R, Kudoh S, Hasegawa K, Niimori-Kita K and Ito T: Notch1 signaling controls cell proliferation, apoptosis and differentiation in lung carcinoma. Lung Cancer 85: 131-140, 2014.
33. Li C, Zhang S, Lu Y, Zhang Y, Wang E and Cui Z: The roles of Notch3 on the cell proliferation and apoptosis induced by CHIR99021 in NSCLC cell lines: A functional link between Wnt and Notch signaling pathways. PLoS One 8: e84659, 2013.
34. Li Z, Xiao J, Liu M, Cui J, Lian B, Sun Y and Li C: Notch3 regulates ferroptosis via ROS-induced lipid peroxidation in NSCLC cells. FEBS Open Bio 12: 1197-1205, 2022.
35. Bakir B, Chiarella AM, Pitarresi JR and Rustgi AK: EMT, MET, plasticity, and tumor metastasis. Trends Cell Biol 30: 764-776, 2020.
36. Zhang YE and Stuelten CH: Alternative splicing in EMT and TGF-β signaling during cancer progression. Semin Cancer Biol 101: 1-11, 2024.
37. Dong C, Wu K, Gu S, Wang W, Xie S and Zhou Y: PTBP3 mediates TGF-β-induced EMT and metastasis of lung adenocarcinoma. Cell Cycle 21: 1406-1421, 2022.
38. Su Q, Wang JJ, Ren JY, Wu Q, Chen K, Tu KH, Zhang Y, Leong SW, Sarwar A, Han X, *et al*: Parkin deficiency promotes liver cancer metastasis by TMEFF1 transcription activation via TGF-β/Smad2/3 pathway. Acta Pharmacol Sin 45: 1520-1529, 2024.
39. Oh MK, Joo H and Kim IS: Prohaptoglobin inhibits the transforming growth factor-β-induced epithelial-to-mesenchymal transition in vitro by increasing Smad1/5 activation and suppressing the Smad2/3 signaling pathway in SK-Hep1 liver cancer cells. PLoS One 17: e0266409, 2022.
40. Su J, Morgani SM, David CJ, Wang Q, Er EE, Huang YH, Basnet H, Zou Y, Shu W, Soni RK, *et al*: TGF-β orchestrates fibrogenic and developmental EMTs via the RAS effector RREB1. Nature 577: 566-571, 2020.
41. Gough NR, Xiang X and Mishra L: TGF-β signaling in liver, pancreas, and gastrointestinal diseases and cancer. Gastroenterology 161: 434-452.e15, 2021.
42. Liu L, Chen X, Wang Y, Qu Z, Lu Q, Zhao J, Yan X, Zhang H and Zhou Y: Notch3 is important for TGF-β-induced epithelial-mesenchymal transition in non-small cell lung cancer bone metastasis by regulating ZEB-1. Cancer Gene Ther 21: 364-372, 2014.
43. Danielpour D, Corum S, Leahy P and Bangalore A: Jagged-1 is induced by mTOR inhibitors in renal cancer cells through an Akt/ALK5/Smad4-dependent mechanism. Curr Res Pharmacol Drug Discov 3: 100117, 2022.
44. Chen WJ, Zhong HT, Wu HT, Hou YY, Wu Z, Fang ZX and Liu J: NOTCH3 inhibits transcription factor ZEB1 expression and metastasis of breast cancer cells via transcriptionally upregulating miR-223. J Cancer 15: 192-203, 2024.
45. Ohashi S, Natsuizaka M, Naganuma S, Kagawa S, Kimura S, Itoh H, Kalman RA, Nakagawa M, Darling DS, Basu D, *et al*: A NOTCH3-mediated squamous cell differentiation program limits expansion of EMT-competent cells that express the ZEB transcription factors. Cancer Res 71: 6836-6847, 2011.
46. Lei ZN, Teng QX, Koya J, Liu Y, Chen Z, Zeng L, Chen ZS, Fang S, Wang J, Liu Y and Pan Y: The correlation between cancer stem cells and epithelial-mesenchymal transition: Molecular mechanisms and significance in cancer theragnosis. Front Immunol 15: 1417201, 2024.
47. Xiu M, Wang Y, Li B, Wang X, Xiao F, Chen S, Zhang L, Zhou B and Hua F: The role of Notch3 signaling in cancer stemness and chemoresistance: Molecular mechanisms and targeting strategies. Front Mol Biosci 8: 694141, 2021.
48. Chang Z, Gao Y, Chen P, Gao W, Zhao W, Wu D, Liang W, Chen Z, Chen L and Xi H: THBS2 promotes gastric cancer progression and stemness via the Notch signaling pathway. Am J Cancer Res 14: 3433-3450, 2024.
49. Zhu Z, Miao L, Li K, Ma Q, Pan L, Shen C, Ge Q, Du Y, Yin L, Yang H, *et al*: A hypothalamic-amygdala circuit underlying sexually dimorphic aggression. Neuron 112: 3176-3191.e7, 2024.
50. Day CP, Merlino G and Van Dyke T: Preclinical mouse cancer models: A maze of opportunities and challenges. Cell 163: 39-53, 2015.
51. Prendergast BJ, Onishi KG and Zucker I: Female mice liberated for inclusion in neuroscience and biomedical research. Neurosci Biobehav Rev 40: 1-5, 2014.

Copyright © 2025 Wang et al. This work is licensed under a Creative Commons Attribution-NonCommercial-NoDerivatives 4.0 International (CC BY-NC-ND 4.0) License.